Dokuz Eylül Üniversitesi Mühendislik Fakültesi Fen ve Mühendislik Dergisi
Dokuz Eylul University Faculty of Engineering Journal of Science and Engineering

Basılı/Printed ISSN: 1302-9304. Elektronik/Online ISSN: 2547-958X

Numerical Investigation of Unsteady Cavity Flow Aeroacoustics by Large Eddy Simulation

Zamana Bağlı Kavite Akışı Aeroakustiğinin Büyük Girdap Simülasyonu ile Sayısal Olarak İncelenmesi

Furkan Coşgun[1*], Sertaç Çadırcı[2]

[1,2] Department of Mechanical Engineering, Istanbul Technical University, Gumussuyu, 34437 Istanbul, TURKEY

Sorumlu Yazar / Corresponding Author *: *: cosgun15@itu.edu.tr

Geliş Tarihi / Received: 12.07.2019 *Araştırma Makalesi/Research Article*
Kabul Tarihi / Accepted: 05.11.2019 *DOI: 10.21205/deufmd.2020226425*

Atıf şekli/ How to cite : COŞGUN, F., ÇADIRCI, S. (2020). Numerical Investigation of Unsteady Cavity Flow Aeroacoustics by Large Eddy Simulation. DEUFMD, 259-269.

Abstract

Flow along a cavity is of special interest for researchers due to the occurrence of free shear layer flow and related high levels of sound and pressure forces. In this study, turbulent flow along an open cavity at a low inlet Mach number (Ma = 0.034) is modelled by Large Eddy Simulations (LES). The velocity profiles at various stations inside the open cavity are compared to available experimental data. It is found that LES results agree with experimental data and detects the transient pressure change in the flow field satisfactorily. Transient pressure data in the flow field is evaluated in acoustic analogy. The noise generated by the cavity is compared with the established Rossiter modes and is found to be reasonable. To create an effect on the sound pressure levels (SPL), a small obstacle with quadrilateral cross section is immersed in the shear layer at three different locations. This causes that the SPL peaks are reduced compared to the case without any obstacle. Thus, cavity-induced noise form specific frequencies are redistributed to high frequency broadband noise as a result of this passive flow control method.
Keywords: *Low Mach number flow, Passive flow control, Acoustics analogy, Rossiter mechanism*

Öz

Bir kavite boyunca akış, serbest kayma tabakası akışının oluşması ve buna bağlı olarak yüksek seviyelerde ses ve basınç kuvvetleri nedeniyle araştırmacılar için özel bir ilgi alanı oluşturmaktadır. Bu çalışmada, düşük Mach sayısındaki (Ma = 0.034) açık bir kavite boyunca türbülanslı akış Büyük Girdap Simülasyonları (LES) ile modellenmiştir. Açık kavite içindeki çeşitli konumlardaki hız profilleri, mevcut deneysel verilerle karşılaştırılmıştır. LES sonuçlarının deneysel verilerle uyuştuğu ve akış alanındaki zamana bağlı basınç çalkantılarını tatmin edici şekilde tespit edebildiği bulunmuştur. Akış alanındaki bu basınç verileri akustik analojide değerlendirilmiştir. Kavitenin ürettiği gürültü, Rossiter modlarıyla karşılaştırılmış ve makul seviyede bulunmuştur. Ses basıncı seviyeleri (SPL) üzerinde bir etki yaratmak için, kesme katmanına üç farklı noktada dörtgen kesitli küçük bir engel daldırılmıştır. Bu, herhangi bir engel olmadığı duruma kıyasla SPL doruklarının azalmasına neden olmaktadır. Bu nedenle, kavite kaynaklı gürültüye özgü frekanslar, bu pasif akış kontrol yönteminin bir sonucu olarak yüksek frekanslı geniş bant gürültüsüne yeniden dağıtılır.
Anahtar Kelimeler: *Düşük Mach sayısı akışı, Pasif akış kontrolü, Akustik analoji, Rossiter mekanizması*

1. Introduction

The flow along a cavity geometry is a highly complex flow type that has been studied by many researchers in the past decades [1]. Cavity flow can be found in many engineering applications.

Cavity flows may be encountered in aircraft landing gear [2], in cargo spaces and load bay on military and commercial airplanes [3], in doorways of automobiles, in spaces in the front and rear windows of automobiles [4] and around high buildings [5]. Cavity geometry encountered in various engineering applications has become a challenging research area which is being studied more and more because it is a source of many different problems such as higher friction forces, excessive noise and vibration. Cavity flow can cause high levels of noises [6] and may damage sensitive devices because of the strong changes in pressure, speed and density. The temporal changes are often followed by aeroacoustics emissions associated with noise generation in different and broad band [7].

The structure of the flow through the open cavity is given in Figure 1. In the cavity flow field, the boundary layer '2' is formed by the interaction of the free stream flow '1' with the front wall of the cavity. Then the shear layer '3' is formed immediately after the cavity front wall. Vortices '4' are separated from the front wall and form big circulation flow regions '6' in the cavity by the interaction with the rear wall of cavity '5'. The time-varying pressure change '7' is fed by the vortex and reverse flow regions, which break away from the front wall and gives rise to acoustic pressure propagation '8'.

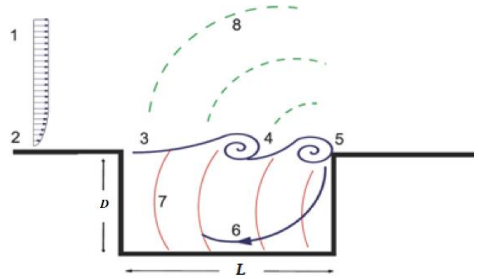

Figure 1. The structure of the flow through the open cavity [8]

The noise spectra are dominated by multiple fluctuations created by pressure distribution with periodic character in most cases, and these fluctuations are followed by the harmonics of the sound pressure level caused by random components with very high time dependence. These fluctuations are called resonance frequencies or cavity tones. These fluctuations are caused by collision between sound propagation and the cavity shear layer in the front wall region. This interaction between the flow field and the acoustical field is an important research area and is widely known as the Rossiter Mechanism [9].

Most of the studies on the cavity flow in the literature have been carried out for supersonic or transonic flows since flows around engineering products such as aircrafts, launchers etc. can be analyzed by high Mach number flows. Aeroacoustics studies on cavity flow at low Mach numbers are rare. Low Mach number cavity flow and its aeroacoustics started to gain attention nowadays to reduce environmental noise levels at urban areas. Landing civil and military aircrafts, automobile's sunroofs, small pillar and submarines with many cavities on the surface are some examples which include low Mach number cavity flow phenomena. Cavity induced noise propagation is an undesired outcome for submarines security and privacy [10]. It is a well-known fact that Rossiter mechanism and modes quite successfully work for relatively high Mach number cavity flows. On the other hand, it is still a question whether relatively low Mach number cavity flows (Ma<0.2) are valid for Rossiter modes and formulas.

Initial experimental studies on the cavity flow were performed by Rossiter (1966) and East (1966). J. E. Rossiter (1966) has conducted experimental studies for six different cavity depths under flow conditions where the Mach number (Ma) varied between 0.4 and 1.2 and the Reynolds number was 2.2×10^6. The time-dependent pressure fluctuations for flat channel flows and cavity flows at various depths and different Ma numbers were compared to reveal their influences on the amplitude spectra. East (1966) demonstrated in an experimental study of open cavities at low Mach numbers that such cavities could produce tones at different frequencies. In addition, the cavity tones only occur when the shear layer interacts with the acoustic propagation [11]. Studies of various active or passive flow control methods applied to the cavity flow for the removal of aeroacoustics effects started in the 1970's.

A pioneering study in this area is done by Heller (1975), and L. L. Shaw (1979). Heller (1975) has performed experimental studies for flows varying between 0.8-5 Mach numbers along rectangular cavities whose aspect ratio change between 2.3 and 5.5 [12]. Experiments that have been performed by tilting the back wall of the cavity have revealed a decrease in the cavity-induced sound levels. Shaw (1979) showed that a ramp placed in the rear wall of the cavity and a velocity cutter placed in the cavity front wall had a positive impact on the cavity-induced sound reduction for both subsonic and supersonic flows [13].

Larcheveque et al. (2004) studied the development of the mixture layer generation throughout the cavity using LES approach. It was shown that while the pressures from the cavity walls gave highly consistent results with the experimental data, an absolute error of 5 dB occurred in the cavity resonance values. It was emphasized that Rossiter modal values of cavity-induced oscillations were independent of the cavity width [14]. Yamouni et al. (2013) studied cavity flow in incompressible and transonic regimes to develop a stability analysis for such flows where they used a cylindrical obstacle in the upstream boundary layer and shear layer. They showed that the flow control with cylinder is effective in reducing the acoustic energy [15].

Zafer et al. (2016 and 2017 and 2018) have conducted three different studies related to low Mach number flows. It is shown that standard k-omega has a superiority compared to SST k-omega and standard k-epsilon to dissolve low Mach number cavity flow among RANS models. Transient pressure inside the cavity from standard k-omega model was used in Ffowcs Williams – Hawkings analogy to determine cavity noise levels. Additionally, a different permeable acoustic source surface which covers the cavity like a reverse box is used to activate quadrupole term of FW-H equation. It is shown that adding a quadrupole term increases sound level in the high frequency range [8]. In 2017, Zafer and Konan studied the effect of cavity – airfoil interaction with passive control on the acoustic signal. It is shown this interaction causes a 20-dB increase in the SPL-Frequency spectrum of 100 Hz while no significant change is observed in low frequency range [16]. In 2018, Zafer and Cosgun studied a cavity geometry other than in [8]. Comparison of various turbulence models used for low Mach number cavity flows showed that DES approach is superior than other RANS models in terms of both flow field and aeroacoustics prediction [17].In the present study, LES simulations are performed for a turbulent flow along a cavity at low Mach number and validated with available experimental data. Aeroacoustics tones obtained by LES are compared to Rossiter modes by the Rossiter formula to test the validity of LES for low Mach number cavity flows. Cavity-induced noise levels have been calculated at different distances from the cavity. The study shows what kind of an effect the passive control of the free shear layer has on the reduction of the SPL peaks.

2. Material and Method

2.1. Numerical modelling

Computations of the flow along a cavity have been carried out using the CFD solver ANSYS-Fluent. The implicit time advancement is used for temporal discretization, while the finite volume approach is used for spatial discretization. Fractional Step algorithm is used to decompose the pressure - velocity coupling in the incompressible flow field solutions. In the spatial discretization, the bounded central difference scheme for momentum is used and in temporal discretization, the Second Order Implicit is used.

The continuity and the Navier Stokes equations employed for LES are obtained by filtering the unsteady governing equations. Eddies whose scales are smaller than the filter width or grid spacing in the CFD simulations are filtered and a filtered variable is denoted by an overbar. Filtering the continuity and momentum equations, Equations (1) and (2) are obtained [20].

$$\frac{\partial \rho}{\partial t} + \frac{\partial}{\partial x_i}(\rho \overline{u_i}) = 0 \tag{1}$$

$$\frac{\partial}{\partial t}(\rho \overline{u_i}) + \frac{\partial}{\partial x_j}\left(\rho \overline{u_i}\,\overline{u_j}\right) = \frac{\partial}{\partial x_j}\left(\sigma_{ij}\right) - \frac{\partial \overline{p}}{\partial x_i} - \frac{\partial \tau_{ij}}{\partial x_j} \tag{2}$$

$$\sigma_{ij} = \left[\mu\left(\frac{\partial \overline{u_i}}{\partial x_j} + \frac{\partial \overline{u_j}}{\partial x_i}\right)\right] - \frac{2}{3}\mu \frac{\partial \overline{u_l}}{\partial x_l}\delta_{ij} \tag{3}$$

$$\tau_{ij} = \rho\overline{u_i u_j} - \rho\overline{u_i}\,\overline{u_j} \quad (4)$$

Where σ_{ij} in Equation (3) is the tensor due to molecular viscosity and τ_{ij} in Equation (4) is the subgrid-scale stress.

Time dependent pressure data taken from flow field solved by LES is used as input in acoustic analogy. Ffowcs Williams-Hawkings equation in Eq. (5a) [18] is solved numerically to predict cavity induced noise level. Ffowcs Williams-Hawkings equation is the most general version of Lighthill acoustic analogy [19] ,which is first proposed to estimate flow induced noise level, but it is only valid when there is no any solid boundary into the flow field.

$$\begin{aligned}\frac{1}{a_0}\frac{\partial^2 p'}{\partial t^2} - \nabla^2 p' = {} & \frac{\partial^2}{\partial x_i \partial x_j}\{T_{ij}H(f)\} \\ & - \frac{\partial}{\partial x_i}\{[P_{ij}n_j + \rho u_i(u_n - v_n)]\delta(f)\} \\ & + \frac{\partial}{\partial t}\{[\rho_0 v_n + \rho(u_n - v_n)]\delta(f)\}\end{aligned} \quad (5a)$$

In Equations (5a-c), u_i is the velocity component of the flow in x_i direction, u_n is the velocity component of the flow in normal direction to the surface. Similarly, v_i is surface velocity component in x_i direction and v_n is surface velocity component in normal direction to the surface. $H(f)$ is Heaviside function, δ_{ij} is Dirac delta function. Lighthill tensor T_{ij}, and compressive stress tensor P_{ij} are given in Equations (5b) and (5c), respectively [20].

$$T_{ij} = \rho u_i u_j + P_{ij} - {a_0}^2(\rho - \rho_0)\delta_{ij} \quad (5b)$$

$$P_{ij} = p\delta_{ij} - \mu\left[\frac{\partial u_i}{\partial x_j} + \frac{\partial u_j}{\partial x_i} - \frac{2}{3}\frac{\partial u_l}{\partial x_l}\delta_{ij}\right] \quad (5c)$$

2.2. Computational domain and boundary conditions

The geometry of the cavity with its dimensions is shown in Figure 2 and it is prepared in accordance to the experimental study [21]. The step height h and the length L of the cavity are taken as 5 mm and 20 mm, respectively. The computational domain starts at $6h$ upstream from leading wall of cavity and ends at $15h$ after the rear wall of the cavity. To ensure a fully developed flow and prevent numerical errors associated with the boundary condition, the channel length downstream of the cavity is taken sufficiently long.

As the inflow boundary condition, uniform velocity at 11.68 m/s is prescribed and the inlet Reynolds is calculated based on this velocity and cavity step height which is 4000 [21]. Zero gradient boundary condition is used at the outlet. Bottom and top channel walls are defined as walls with no slip boundary condition and the lateral sides of the channel are assumed to satisfy symmetry boundary condition. The inlet Mach number is around 0.034 and the flow is assumed to be incompressible. The constant thermo-physical properties of the air such as the density and viscosity are at standard atmospheric conditions.

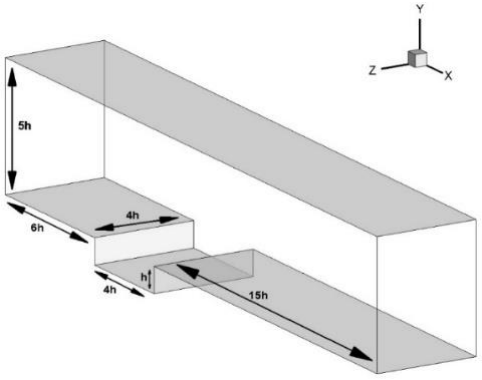

Figure 2. Dimensions of the 3D flow domain

3. Results

3.1. Mesh convergence tests

Five different orthogonally structured meshes are used in the mesh convergence tests. Figure 3 shows details about the mesh structure which is determined as the adequate mesh with nearly 3.3 million cells after mesh convergence tests. Figure 4 shows the mesh convergence results evaluated by time-averaged pressure values obtained from a receiver at a critical location in the free shear layer. As a result, the adequate mesh with nearly 3.3 million cells is used in calculations.

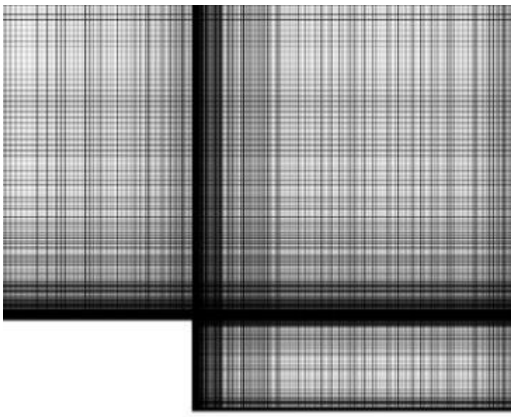

Figure 3. Mesh structure with nearly 3.3 million cells

Time dependent pressure fluctuations are provided from a receiver located inside the cavity (x=0.005, y=0, z=0). The time history of the pressure acquired from the receiver is shown in Figure 5. Time-averaging of the pressure values is done after quasi-steady flow characteristics were observed at 0.05 seconds. Simulation time is taken sufficiently short because the geometry is small, and the speed is relatively high. The simulation time corresponds to 6-7 periods where in one period the fluid reaches the outlet of the domain.

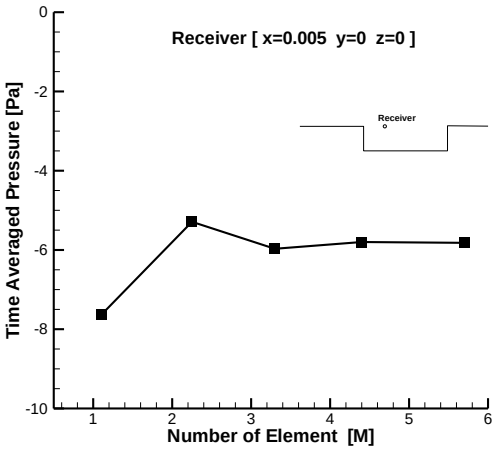

Figure 4. Time averaged pressure vs. number of cells

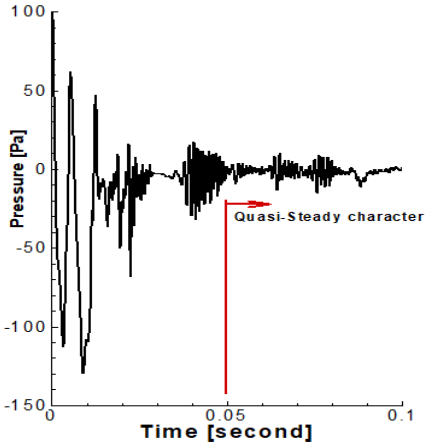

Figure 5. Time history of pressure fluctuations

3.2. Computational settings

The conservation equations are implicitly decomposed using the finite volume method, and the matrices in algebraic form are solved by using Algebraic Multiple Grid (AMG solver) with sub-iterations for each time step. Non-iterative closed solver is used for time advancement in the current study. This solver computes the iteration errors until the convergence criteria are satisfied without using outer iterations that increase the computational demand for each time step [22]. The convergence criteria are set to 10^{-6} for both momentum and continuity equations. Maximum number of inner iterations are defined as 10 and 20 for momentum and continuity equations, respectively. The least square cell-based method is used to solve the secondary fluxes. The fixed time step is set to 10^{-5} seconds [8]. The simulations are proceeded till 0.1 seconds as displayed in Figure 5 since the flow becomes quasi-steady after 0.05 seconds.

After the computational settings have been determined for the selected mesh, the base flow is solved which yields a wall y^+ distribution as demonstrated in Figure 6. The averaged y^+ values inside the cavity and in downstream direction are below 1.

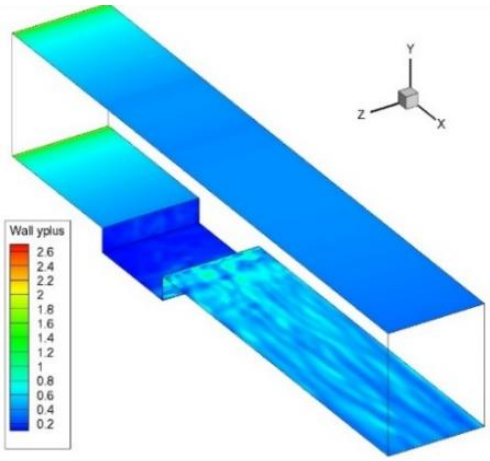

Figure 6. Wall y+ distributions for the selected mesh

3.3. CFD results for the base flow and validation

After intensive mesh convergence tests, the numerical results are compared with experimental data for validation. To be able to make a robust comparison between current CFD results and PIV measurements, the stations of cavity-inside velocity profiles are determined as given by Ozsoy in 2010 [21].

Figure 7 represents the comparison of the time-averaged *u*-velocity profiles with the experimental data. The velocities are rendered dimensionless with the inlet velocity, 11.68 m/s. The time-averaged velocity profiles obtained from LES solutions provide excellent agreements with the experimental data although there are some small deviations caused by the complexity of the shear layer flow behavior.

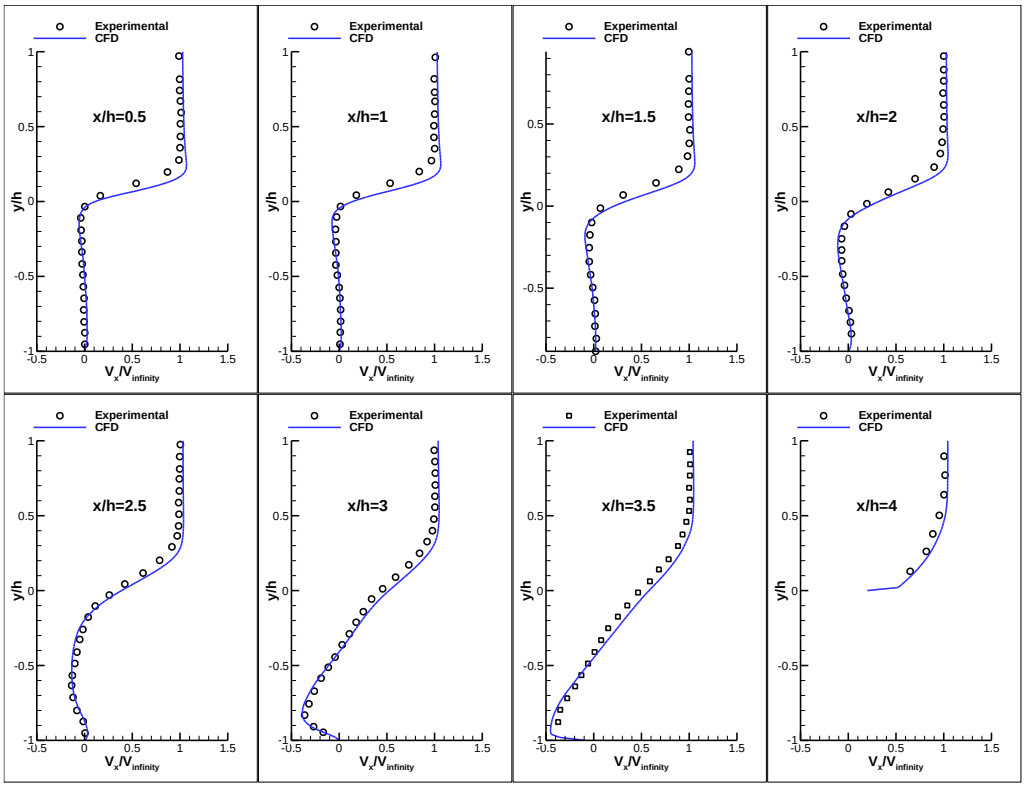

Figure 7. Time averaged u-velocity profiles inside the cavity

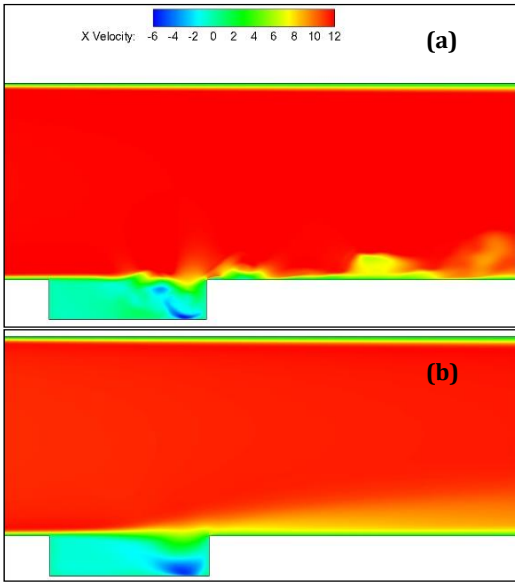

Figure 8. u-velocity contour at the mid-plane for (a) instantaneous time at t = 0.1 s., (b) time-averaged field

Figures 8a and 8b show instantaneous and time-averaged u-velocity contours, respectively. Figure 8a shows the shear layer generating at the leading edge of the cavity which becomes unstable and oscillates significantly downstream of the cavity. This physical phenomenon is known as shear layer thickening along the cavity as can be demonstrated in the time-averaged flow field in Fig. 8b.

The shear layer flow affects the rear corner of the cavity wall. The occurrence of the high pressure in the close vicinity of the cavity's rear corner is a result of the impingement of the strong shear layer with the rear wall of the cavity. This explains the generation of high temporal gradients of pressure and these high-pressure changes cause sound pressure propagation throughout flow field.

3.4. Aeroacoustics results for the base flow

The cavity-induced sound pressure values are calculated by Ffowcs Williams Hawkings relation in Equation (5a) and they are converted to sound pressure level (SPL) in the frequency domain with Fast Fourier Transform (FFT) that is given in Equation (6).

The lowest frequency value is 10 Hz and the highest frequency is 5000 Hz. Sampling time step is identified as 10 where sampling interval of FFT is 10^{-4} seconds. Hamming's window is used as window function which is provided by ANSYS-Fluent flow solver.

$$SPL = 20\ log\left(\frac{p'_{RMS}}{p_{ref}}\right), p_{ref} = 2x10^{-5} \quad (6)$$

Here, p_{rms} represents root mean square value of transient pressure changes in related time interval while p_{ref} is the reference sound pressure.

In the present study, twenty virtual microphones are distributed on quarter-circles to receive sound pressures around the cavity, as shown in Figure 9. All microphones are on the mid-plane of the flow domain. Each quarter circle indicates a certain microphone series from 1 to 5.

Figure 10a shows the SPL spectra for the microphone series around the cavity. It can be seen that some frequencies behave dominantly, and other frequencies are their sub-harmonics. At all distances, the highest noise level is encountered at the second peak corresponding to nearly 300 Hz. Cavity-induced noise levels decrease inherently while moving away from the cavity region, but SPL spectrum indicates almost the same behavior due to low dissipative character of sound. Figure 10b indicates that three dominant modes govern the sound spectrum for Series-1. The SPL peaks are at 155.6 Hz, 311.2 Hz and 466.8 Hz for the first, second and third modes, respectively.

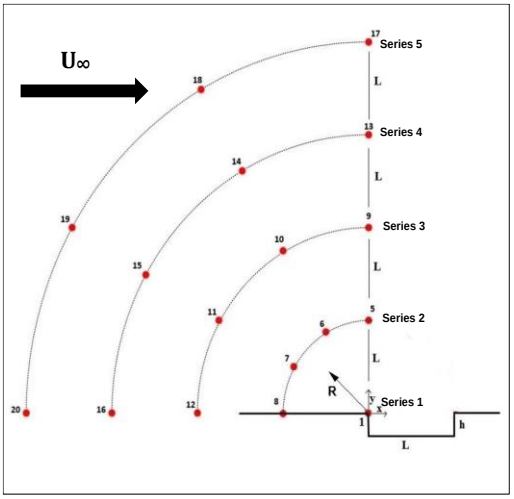

Figure 9. Locations of the virtual microphones

Rossiter is a pioneering researcher who suggested an empirical formula (Equation 7) which provides dominant frequencies created by self-sustained cavity oscillations [9].

Calculated modes in a former study [8] can be associated with the modes in Figure 10b. The results in the present study have proven, that Rossiter formula successfully estimates cavity tones and is valid for low Mach number cavity flows.

In Equation (7), m is corresponding to Rossiter frequency's mode index. U is the incoming free stream velocity magnitude and Ma is the Mach number of the free stream. Phase delay of two vortices separating at the leading wall of cavity is symbolized by α. κ is defined as ratio of vortex convective speed to free stream velocity magnitude [8].

$$f_m = \frac{U}{L}\frac{m-\alpha}{M+\frac{1}{\kappa}} \tag{7}$$

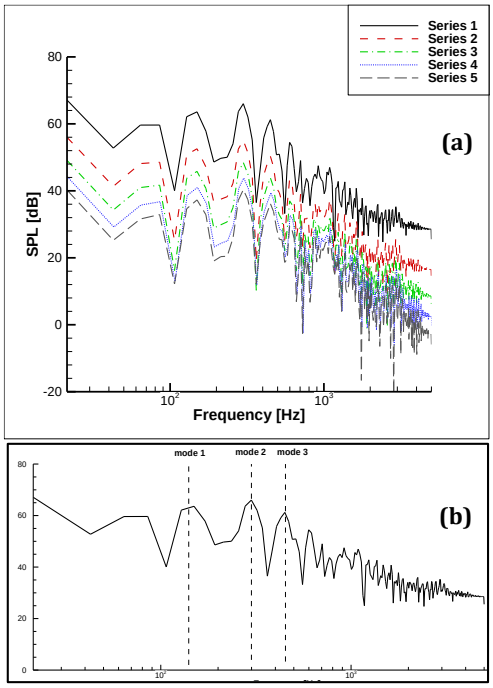

Figure 10. SPL spectra (a) for of all microphone series, (b) for series 1

To indicate the details of the eddies past the cavity, the flow field is visualized with iso-surfaces past the cavity as shown in Figure 11. It should be pointed out that the aeroacoustics behavior can be analyzed if the generation of the eddies is modeled appropriately.

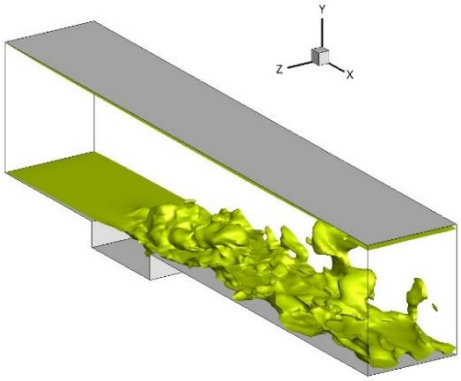

Figure11. Iso-surfaces of the flow past the cavity

3.5. Aeroacoustics results for the cases with an obstacle

To suppress the peaks of SPLs inside the cavity, an obstacle is located into the shear layer flow at three different locations in a distance of h, $2h$ and $3h$ from the front corner of the cavity, separately. In the cavity flows, it is known that cavity rear wall – shear layer interaction is the main reason for sound propagation. The purpose of immersing a thin obstacle into the shear layer region is to inhibit this interaction and suppress sound generation mechanism in the cavity. Figure 12 shows the locations of the obstacles with quadrilateral cross sections. One edge of the obstacle is 10 % of the cavity height h. The obstacle is chosen with quadrilateral cross section which fits to structured mesh appropriately. Furthermore, the effect of the obstacle's shape is not considered as a parameter in the study.

Immersing a very thin obstacle into the shear flow causes the separation of the shear layer flow. As a result, the vortex structure is distributed before the shear flow reaches the rear wall of the cavity as seen in Figure 13. An alternation in the flow field will also influence the acoustic behavior of the flow. If the obstacle is closer to the front wall or leading edge of the cavity, the detachment will be initiated earlier, hence, the main vortex structure in the rear region of the cavity will be deteriorated and this will influence the reduction of the SPL peaks. The closest character to the reference case is shown by Obstacle 3. These results reflect almost the same sound spectrum behavior of the reference case in not only Rossiter mode frequencies but also in the high frequency region.

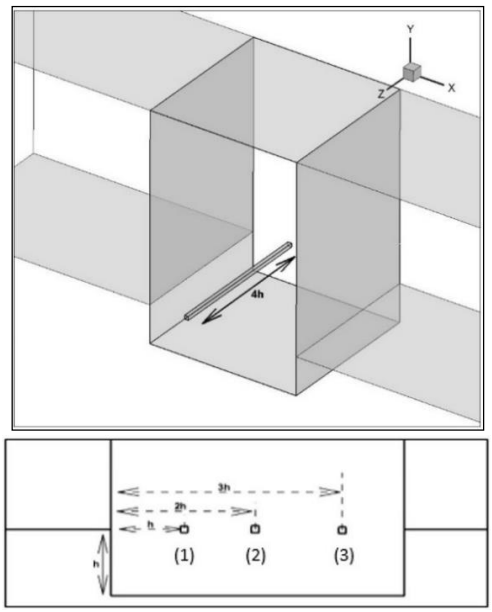

Figure 12. Obstacle locations inside the cavity

If the frequency spectra are dominated by high-amplitude tones rather than broad band discrete tones, the objective in controlling the sound level is mainly reducing the resonances. In the current study SPL values at only dominant frequencies are reduced by immersing a thin obstacle in the cavity.

Figure 14 compares SPL spectra of the reference case and spectra of the cases with obstacles, calculated in Series 5. Obstacle 1 provides better results in term of SPL peak reduction compared to the other obstacles. The benefit of using this obstacle can be observed in the SPL reduction of 6 decibels in the first Rossiter mod and 10 decibels in the second and third Rossiter mods, respectively. Despite better results for obstacle 1, in high frequency region sound spectrum is almost identical to the reference case's sound spectrum behavior. It can be said that Obstacle 1 does not have an influence on high energy structures. Obstacle 2 provides a reduction of almost 5 decibels in the sound level, but it gives rise to an extra peak in high frequency region. On the other hand, this one creates an extra resonance in high frequency regions, especially in the tonal range between 1000 Hz to 2000 Hz. When looking at the flow field contours in Figure 13 and SPL spectra in Figure 14, it can be seen that the earlier distributed shear layer, the more reduction in sound level at critical frequency points could be achieved.

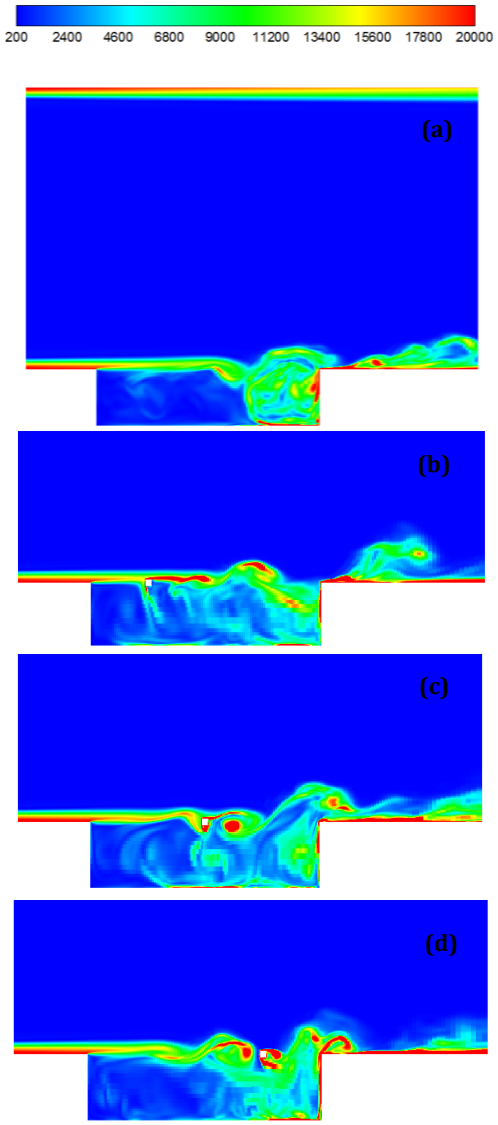

Figure 13. Vortex contours for the cases at t = 0.1s (a) without obstacle (b) obstacle 1 (c) obstacle 2 (d) obstacle 3- colors denote the direction of rotation

In Figure 13b, obstacle 1 causes early distortion of the shear layer hence the impact of vorticity near the rear cavity wall is suppressed. This situation is directly related to tone level reduction on Mode-1, 2 and 3 which can be seen in Figure 14a. A similar situation is observed for obstacle 2 in Fig. 14b which provides a reduction at mode frequency points, but this reduction is less than compared to those by obstacle 1. Finally, for obstacle 3 there is no significant changes in the spectra as shown in

Figure 14c. This is thought that the flow fields are not influenced by obstacle 3 and frequency spectra remains almost indifferent as in the reference case.

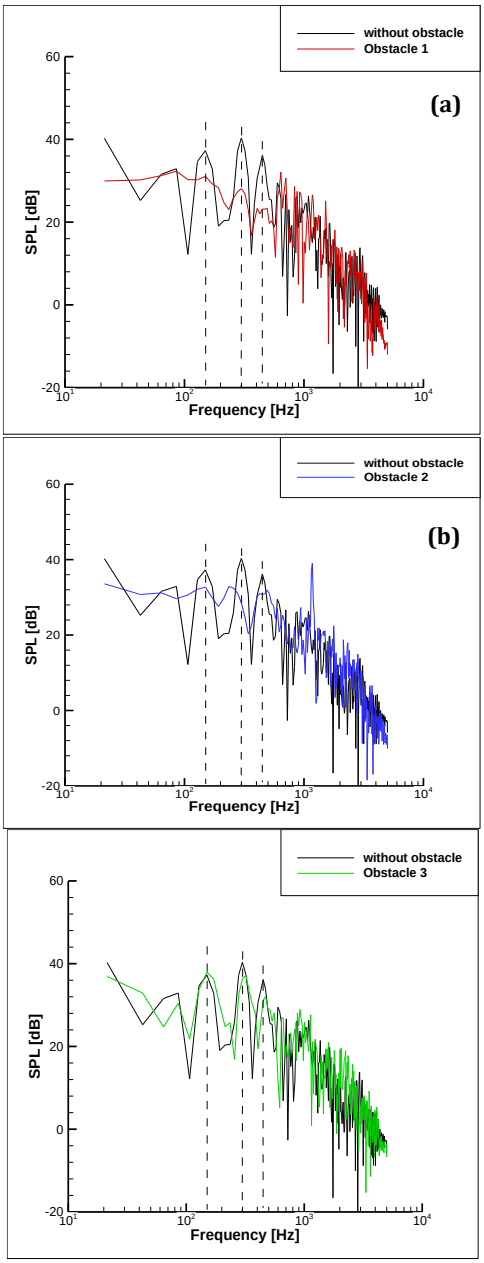

Figure 14. SPL spectra in series 5: Aeroacoustics comparison of the base flow with obstacles (a) 1, (b) 2 and (c) 3

4. Discussion and Conclusion

In the present study, a numerical study was conducted to investigate cavity-induced aeroacoustics behavior by LES simulations. Detailed mesh independency and validation tests were carried out to obtain robust numerical results. To reduce the SPL level peaks, obstacles were immersed into the shear layer flow. In the aeroacoustics investigation, flow induced noise was calculated by Ffowcs Williams Hawkings analogy. It was observed that modal values calculated by the Rossiter relation overlapped with modal values obtained with numerical calculation. The cavity-induced SPLs were around 65 decibels in the near field and around 40 decibels in the far field of the cavity.

Obstacle 1 which is near the leading edge of the cavity provided a noise reduction of 6 decibels in the first Rossiter mod and a noise reduction of 10 decibels in the second and third modes, respectively. Obstacle 2 generated extrinsic resonance values at higher frequencies with higher energies, while obstacle 3 was visibly not effective in the acoustic field. It was concluded that immersing a tiny obstacle into the free shear layer past a cavity might be beneficial in terms of cavity-induced noise reduction in the low frequency region. With this passive flow control, cavity-induced noise has been redistributed from specific frequencies to high frequency broadband noise and the SPL peaks were reduced.

References

[1] Crook, S.D., Lau, T.C.W., Kelso, R.M. 2013. Three-Dimensional Flow within Shallow-Narrow Cavities, Journal of Fluid Mechanics, Vol. 735, pp. 587–612. DOI: 10.1017/jfm.2013.519

[2] Lopez. L.V. 2010. Prediction of Landing Gear Noise Reduction and Comparison to Measurements. 16th AIAA/CEAS Aeroacoustics Conference, Hampton, USA.

[3] Lopez. L.V. 2009. A New Approach to Complete Aircraft Landing Gear Noise Prediction. The Pennsylvania State University, PhD Thesis, Pennsylvania, USA.

[4] Nouzawa. T., Li. Y., Kasaki. N., Nakamura. T. 2011. Mechanism of Aerodynamic Noise Generated from Front-Pillar and Door Mirror of Automobile, Journal of Environment and Engineering, Vol. 6, Issue 3, pp. 615–626. DOI: 10.1299/jee.6.615

[5] Li. G. 2015. Numerical Simulation of Environmental Flow over Buildings for Renewable Energy Application. Arizona State University, Master Thesis, Arizona, USA.

[6] Sarohia. V., Massier. P.F. 1977. Control of Cavity Noise, Journal of Aircraft, Vol. 14, pp. 833–837. DOI: 10.2514/3.58862

[7] Cattafesta, L.N., Song, Q., Williams, D.R., Rowley, C.W., Alvi, F.S. 2008. Active Control of Flow-Induced Cavity Oscillations, Progress in Aerospace Science, Vol. 44, pp. 479–502. DOI: 10.1016/j.paerosci.2008.07.002

[8] Zafer. B., Cosgun. F, 2016. Aeroacoustics Investigation of Incompressible Unsteady Cavity Flow, ", Journal of The Faculty of Engineering and Architecture of Gazi University, Vol. 31-3, pp. 665–675. DOI: 10.17341/gummfd.34239

[9] Rossiter. J. 1966. Wind-Tunnel Experiments on the Flow over Rectangular Cavities at Subsonic and Transonic Speeds, Aeronautical Research Council Reports and Memoranda, London, England.

[10] Basovsky. V.G., Gorban. I.M., Khomenko. O.V. 2018. Modification of Hydrodynamic and Acoustic Fields Generated by a Cavity with Fluid Suction, Modern Mathematics and Mechanics, Chapter 9, pp 137-158.

[11] East. L.F. 1966. Aerodynamically Induced Resonance in Rectangular Cavities, Journal of Sound and Vibration, Vol. 3, pp. 277–287. DOI: 10.1016/0022-460X(66)90096-4

[12] Heller. H.H., Bliss. D.B. 1975. The Physical Mechanism of Flow-Induced Pressure Fluctuations in Cavities and Concepts for Their Suppression. AIAA 2nd Aero-Acoustics Conference, Hampton, USA.

[13] Shaw. L.L. 1979. Suppression of Aerodynamically Induced Cavity Pressure Oscillations, The Journal of the Acoustical Society of America 62, S80, Vol. 62. DOI: 10.1121/1.2016395

[14] Larchevêque. L., Sagaut. P., Comte. P. 2004. Large Eddy Simulation of A Compressible Flow in A Three-dimensional Open Cavity at High Reynolds Number, Journal of Fluid Mechanics, Vol. 516, pp. 265–301. DOI: 10.1017/S0022112004000709

[15] Yamouni. S., Mettot. C., Sipp. D., Jacquin. L. 2013. Passive Control of Cavity Flows, Journal of Aerospace Lab, Issue 6.

[16] Zafer. B., Konan. O. 2017. Aeroacoustic Analysis of Cavity – Airfoil Interaction, Dokuz Eylul University-Faculty of Engineering Journal of Science and Engineering, Vol. 19, pp. 279-294. DOI: 10.21205/deufmd. 2017195523

[17] Zafer. B., Cosgun. F. 2018. Aeroacoustics Analysis of Cavity Flow, Journal of Thermal Science and Technology, Vol. 38-2, pp 25-38.

[18] Ffowcs Williams. JE., Hawkings. D. 1969. Sound Generation by Turbulence and Surfaces in Arbitrary Motion, Philosophical Transactions of The Royal Society of London Series A, Mathematical-Physical and Engineering Sciences, Vol. 264, pp. 321–342 . DOI: 10.1098/rsta.1969.0031

[19] Lighthill. M.J. 1951. On Sound Generated Aerodynamically I. General Theory, Philosophical Transactions of The Royal Society of London Series A, Mathematical-Physical and Engineering Sciences, Vol. 211, pp. 564-587. DOI: 10.1098/rspa.1952.0060

[20] Ansys Inc. 2013. Fluent Theory Guide.

[21] Ozsoy. E. 2010. Numerical Simulation of Incompressible Flow Over Three-Dimensional Rectangular Cavity, Istanbul Technical University, Graduate School of Science Engineering and Technology, PhD Thesis, Istanbul, Turkey.

[22] Cosgun, F. 2018. Aeroacoustics Investigation of Low Mach Number Cavity Flow. Istanbul Technical University, Graduate School of Science Engineering and Technology, Master Thesis, 119p, Istanbul, Turkey.